MICROSCOPY

Microscopy, 2020, 176–182
doi: 10.1093/jmicro/dfaa008
Advance Access Publication Date: 25 March 2020

Letter

Lensless Fourier transform electron holography applied to vortex beam analysis

Ken Harada[1,*], Yoshimasa A. Ono[1] and Yoshio Takahashi[2]

[1]CEMS, RIKEN (The Institute of Physical and Chemical Research), Hatoyama, Saitama 350-0395, Japan and [2]Research and Development Group, Hitachi, Ltd., Hatoyama, Saitama 350-0395, Japan

*To whom correspondence should be addressed. E-mail: kharada@riken.jp

Received 9 January 2020; Revised 2 February 2020; Editorial Decision 16 February 2020; Accepted 18 February 2020

Abstract

Lensless Fourier transform holography has been developed. By treating Bragg diffraction waves as object waves and a transmitted spherical wave as a reference wave, these two waves are interfered and recorded as holograms away from the reciprocal plane. In this method, reconstruction of holograms requires only one Fourier transform. Application of this method to analyze vortex beams worked well and their amplitude and phase distributions were obtained on the reciprocal plane. By combining the conventional holography with the developed lensless Fourier transform holography, we can reconstruct and analyze electron waves from the real to reciprocal space continuously.

Key words: lens-less Fourier transform holography, electron holography, reciprocal space, vortex beam, spherical wavefront, helical wavefront

Electron holography [1,2] is one of the most powerful tools to detect wave properties of electron beams in terms of amplitudes and phases. When electron beams pass through specimens, electron holography can analyze properties of specimen materials, such as inner potentials [3], magnetization [4] and electric charges [5]. In an ordinary image holography method, electron holograms are characterized by specimen images and interference fringes superimposed on the images. Here, observations and analyses of the specimen images are performed in the real space. On the other hand, electron holography in the reciprocal space is rare and only one example has been realized in the Fraunhofer region by using an asymmetric double slit [6].

Fourier transform holography [7] is another technique using the reciprocal space, where a reference wave is a spherical wave whose source is positioned in the same plane as that of observation targets or specimens. Then, interferograms with the object and reference waves are recorded in the angular patterns created by these two waves. This method has an advantage that reconstructions from the interferograms can be realized by only one Fourier transform step. Since recording interferences between the object and reference waves are realized without using a lens system, this technique is called lensless Fourier transform holography. Only one application has been reported in electron microscopy where an amorphous carbon thin film was used as diffusion plate [8]. Even in the X-ray field, only the idea of using a zone plate with a hole has been introduced [9].

In the present study, for realization of the lens-less Fourier transform electron holography, we used vortex beams generated by using a fork-shaped grating [10] in the reciprocal plane as object waves and a transmission wave propagating along the optical axis as a reference wave. These waves were superimposed and interfered as holograms at displaced positions above the reciprocal plane as underfocus holograms and below the reciprocal plane as overfocus holograms.

Figure 1 shows a schematic diagram of the optical system of lensless Fourier transform holography for electron vortex-beam experiments. A fork-shaped grating [10], which is not shown in Fig. 1, for generating vortex beams is irradiated by an incident electron wave. In conventional vortex-beam observations, one of the crossover positions as the reciprocal plane in the imaging optical system is chosen, and diffraction patterns with typical annular ring-shaped spots are observed [11]. In the electron holography for the vortex beams, electron waves passed around the fork-shaped grating are used as reference waves. The 0^{th} order transmission wave spreads out along the optical axis and Bragg diffraction waves from the grating propagate in their flowing direction. Then, the transmission wave and diffraction waves are superimposed above and below the

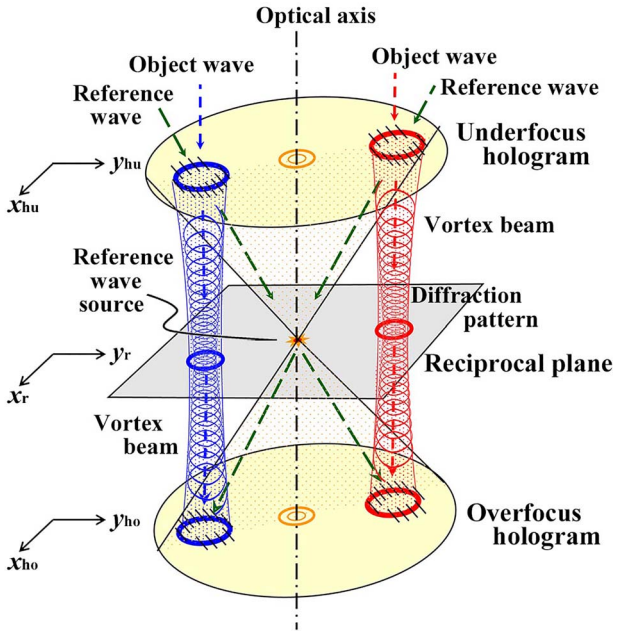

Fig. 1. Schematic diagram of the present experimental setup and for explanation of the relations between object waves and a spherical reference wave. Two vortex beams (blue and red) from a fork-shaped grating as object waves generate annular ring-shaped diffraction spots at the reciprocal plane and a transmitted wave as the reference wave (green) generates a source spot just on the optical axis between the ring spots. Because the spherical wave spreads out and superimposes with the vortex beams above and below the reciprocal plane, both underfocus and overfocus holograms can be recorded in the lensless Fourier transform holography.

reciprocal plane [12,13]. The two-wave interference patterns are recorded as holograms, such as underfocus holograms and overfocus holograms. This is the holography system in the reciprocal space in which diffraction waves correspond to object waves, and the 0^{th} order wave corresponds to a reference wave. Furthermore, the source of the reference wave is positioned in the same plane as that of the objects, indicating the annular ring-shaped diffraction waves as vortex beams. The interference occurs between vortex beams and spherical waves from the reference wave source. Then, the interference patterns are recorded with the angular relation between the waves. This simple interference method is suitable for reconstruction of the holograms of the vortex beams in the reciprocal plane.

We explain the angular relation shown in Fig. 1; the red and blue arrows are vortex beams in the respective diffraction spot, and green arrows are reference waves for vortex beams above and below the reciprocal plane. For example, in the underfocus holograms, the reference wave is superimposed on the left annular diffraction spot from the left-hand side, and the reference wave is superimposed on the right annular diffraction spot from the right-hand side. On the contrary, in the overfocus holograms, the reference wave is superimposed on the left annular diffraction spots from the right-hand side, and the reference wave is superimposed on the right annular diffraction spots from the left-hand side. In this way, their angular relations are exchanged.

Here, we explain procedures of the Fourier transform holography by using equations. One of the vortex beams generated by the fork-shaped grating as the objective wave at the reciprocal plane is described by $\varphi_{obj}(x_r, y_r)$ given by

$$\varphi_{obj}(x_r, y_r) = \phi_{obj}(x_r, y_r)\exp\left[i\eta_{obj}(x_r, y_r)\right] \tag{1}$$

where ϕ_{obj} is an amplitude distribution and η_{obj} is a phase distribution at the reciprocal plane, and (x_r, y_r) indicates coordinates in the reciprocal plane. The object wave propagates a large optical distance from the reciprocal plane to the hologram-recording plane whose coordinates are described by (x_h, y_h), where the wave can be described as a Fraunhofer diffraction wave $\Psi_{obj}(x_h, y_h)$ through Fourier transformation given by

$$\begin{aligned}\Psi_{obj}(x_h, y_h) &= F\left[\varphi_{obj}(x_r, y_r)\right](x_h, y_h)\\ &= F\left[\phi_{obj}(x_r, y_r)\exp\left[i\eta_{obj}(x_r, y_r)\right]\right](x_h, y_h)\end{aligned} \tag{2}$$

We consider a plane wave slightly tilted to the x_h direction as the reference wave $\Psi_{ref}(x_h, y_h)$ in the hologram-recording plane given by

$$\Psi_{ref}(x_h, y_h) = \phi_{ref}(x_h, y_h)\exp\left[iR_h x_h\right] \tag{3}$$

where R_h (= $\sin(\alpha)/\lambda$) is the spatial frequency in terms of the tilt angle of the reference wave α and the wavelength λ, and $\phi_{ref}(x_h, y_h)$ is the amplitude of the reference wave taken to be unity. When the object and reference waves are superimposed and interfered in the hologram-recording plane, their intensity distribution $II_{holo}(x_h, y_h)$ is recorded as the Fourier transform hologram described by the following equation:

$$\begin{aligned}II_{holo}(x_h, y_h) &= \left|\Psi_{obj}(x_h, y_h) + \Psi_{ref}(x_h, y_h)\right|^2\\ &= 1 + \left|\Psi_{obj}(x_h, y_h)\right|^2\\ &+ F\left[\phi_{obj}(x_r, y_r)\exp\left[i\eta_{obj}(x_r, y_r)\right]\right]^*(x_h, y_h) \times \exp\left[iR_h x_h\right]\\ &+ F\left[\phi_{obj}(x_r, y_r)\exp\left[i\eta_{obj}(x_r, y_r)\right]\right](x_h, y_h) \times \exp\left[-iR_h x_h\right],\end{aligned} \tag{4}$$

where the asterisk * indicates a complex conjugate. When we take Fourier transform of the intensity distribution $II_{holo}(x_h, y_h)$, we can simultaneously obtain two reconstructed waves as described in the following equation:

$$\begin{aligned}F\left[II_{holo}(x_h, y_h)\right](x_r, y_r) &= F\left[1 + \left|\Psi_{obj}(x_h, y_h)\right|^2\right](x_r, y_r)\\ &+F\left[F\left[\phi_{obj}(x_r, y_r)\exp\left[i\eta_{obj}(x_r, y_r)\right]\right]^*(x_h, y_h)\right.\\ &\quad\left.\times\exp\left[iR_h x_h\right]\right](x_r, y_r)\\ &+F\left[F\left[\phi_{obj}(x_r, y_r)\exp\left[i\eta_{obj}(x_r, y_r)\right]\right](x_h, y_h)\right.\\ &\quad\left.\times\exp\left[-iR_h x_h\right]\right](x_r, y_r)\\ &= F\left[1 + \left|\Psi_o(x_h, y_h)\right|^2\right](x_r, y_r)\\ &+\phi_o(x_r - R_h, y_r)\exp\left[i\eta(x_r - R_h, y_r)\right] + \phi_o(-x_r - R_h, -y_r)\\ &\quad\exp\left[-i\eta(-x_r - R_h, -y_r)\right].\\ &= F\left[1 + \left|\Psi_o(x_h, y_h)\right|^2\right](x_r, y_r) + \varphi_o(x_r - R_h, y_r)\\ &\quad+\varphi_o{}^*(-x_r - R_h, -y_r).\end{aligned} \tag{5}$$

The first term of Eq. (5) represents the background intensity distribution; the second and third terms correspond to the two

reconstructed waves, i.e. the object wave and its conjugate wave. Equation (5) explains that the two reconstructed waves are displaced from the position of the optical axis depending on the tilt angle α of the reference wave in Eq. (3). We can use both waves for analyses of wave properties.

Fork-shaped gratings made of Si_3N_4 membrane 150 nm thick including the third-ordered edge dislocations were fabricated using a focused ion beam instrument (NB-5000, Hitachi High-Technologies Corp.). The size of the grating opening was 5 μm in diameter, and the irradiation area by the incident electron beam was about 50 μm in diameter, which is about 10 times larger than the grating opening. Since the beam irradiation area is large, the transmitted beam around the grating was spread out quickly after passing through the reciprocal plane and superimposed with the diffracted waves as the vortex beams on both sides of the 0^{th} order beam. Therefore, the obtained hologram is of a wavefront splitting type, which is the same as that of the conventional electron holography. The optical system for the experiment was the same as that for observation of small angle electron diffraction (SmAED) patterns [14] at the camera length of about 710 m. The vortex beams and their holograms were observed with a 300-kV field emission transmission electron microscope (HF-3300S, Hitachi High-Technologies Corp.).

Figure 2 shows relationships between spherical wavefronts and helical wavefronts of vortex beams and the direction of the azimuthal rotation of the vortex structures around the vortex beams; (a) the left-hand side circular spot above the reciprocal plane, (b) the right-hand side spot above the reciprocal plane, (c) the left-hand side spot below the reciprocal plane and (d) the right-hand side spot below the reciprocal plane. The upper parts in Fig. 2 show overlaps of helical wavefronts of vortex beams and spherical wavefronts above and below the reciprocal plane. Phase gradients of vortex beams are shown at the upper parts as the intersections of two wavefronts, and intersections represent interference fringes in the holograms. When the shapes of both wavefronts, the vortex beam and the 0^{th} order transmitted wave, are inverted, the spatial relationship between the two wavefronts does not change, and as a result, the interference fringes represented by the intersection of the two wavefronts show the same pattern. The lower parts indicate directions of azimuthal rotations of the vortex structure around the vortex beam, showing vortex-like interference behavior seen from center to outer area: (a) clockwise, (b) counter clockwise, (c) counter clockwise and (d) clockwise. These relations can well explain the reconstructed wavefronts in each hologram as we discuss later.

Figure 3 shows diffraction patterns of vortex beams under five focusing conditions in the optical setup. Figure 3c shows a diffraction pattern on both sides with the first and second order diffraction waves from the fork-shaped grating. The annular ring-shaped spots are typical in the vortex beam observation, and the ring diameter increases with the order of diffraction. The topological numbers of the generated vortex beams are −6, −3, 0, +3, and +6, from left to right. The 0th order Bragg diffraction spread out along propagation directions and then is superimposed with the first and/or second order Bragg diffraction waves; Fig. 3b and d show results for the first-order case, and Fig. 3a and e show results for both the first- and second-order case. We used defocused diffraction pattern in (a) as underfocus holograms and in (e) as overfocus holograms for the lensless Fourier transform holography. The faint ripple-like images on these figures are Fresnel images of carbon fine particles adhered on the fork-shaped grating. Since the positions of the faint Fresnel images on the hologram are spatially separated from the diffraction spots, the reconstructed images of the vortex beams are not affected.

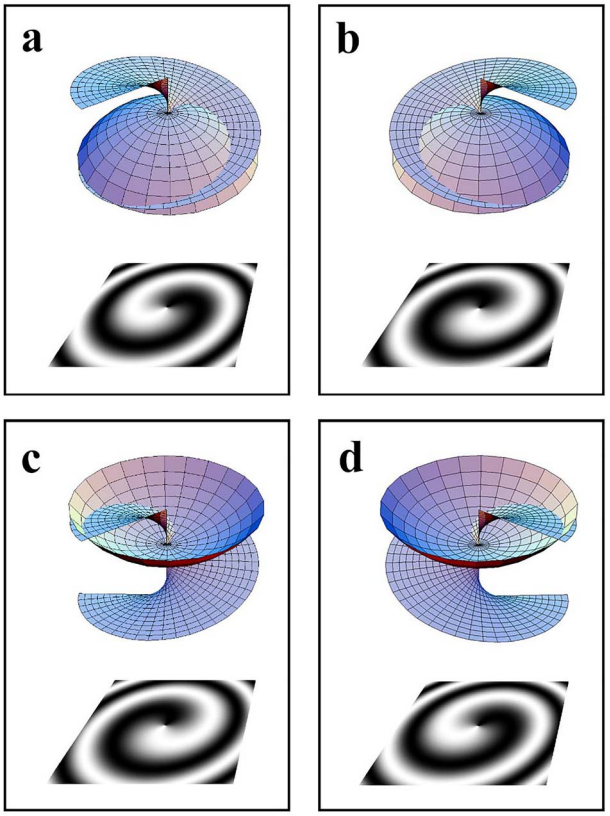

Fig. 2. Schematics showing relations between a spherical wavefront of the reference wave and a helical wavefront of the vortex beam in the upper parts and the direction of the azimuthal rotation of the vortex-structure around the vortex beam in the lower parts. (a) and (b): concave spherical waves above the reciprocal plane with oppositely rotating vortex beams; (c) and (d): convex spherical waves below the reciprocal plane and the same vortex beams of (a) and (b). Wavefronts in (a) and (d) are in conjugate with each other, and (b) and (c) are similarly in conjugate. The gradient of the reconstructed phase images and vortex-structure around the vortex beam are explained using these panels.

Figure 4a shows the same underfocus hologram in Fig. 3a with categorized diffraction spots in red broken squares for Fig. 4b–e. The upper parts in Fig. 4b–e show amplitude images, and the lower parts show phase images. These amplitude and phase images were reconstructed by only one Fourier transformation. Figure 4f and g show composite images of amplitude and phase images for the first and second order diffraction spots. The phase distributions were shown in the color-code representation and combined with the amplitude distributions shown in the luminance representation. The each amplitude image in Fig. 4 corresponds to the vortex beams of the first or second order spots in the reciprocal plane shown in Fig. 3c. The phase image in Fig. 4c shows the fan-like structures with three wings corresponding to the topological number 3 of the vortex beam and is consistent with the results obtained by the conventional electron holography [12,13]. This image, however, shows the phase distribution of the vortex beam in the reciprocal space, which has never been observed before. The relation between the object and conjugate images in Fig. 4c is explained by the angular setup in Fig. 1. Since in the underfocus holograms on the left-hand side, the reference wave (green arrow) is superimposed with the object wave of the vortex beam (blue arrow) irradiated from upper-left, we define the

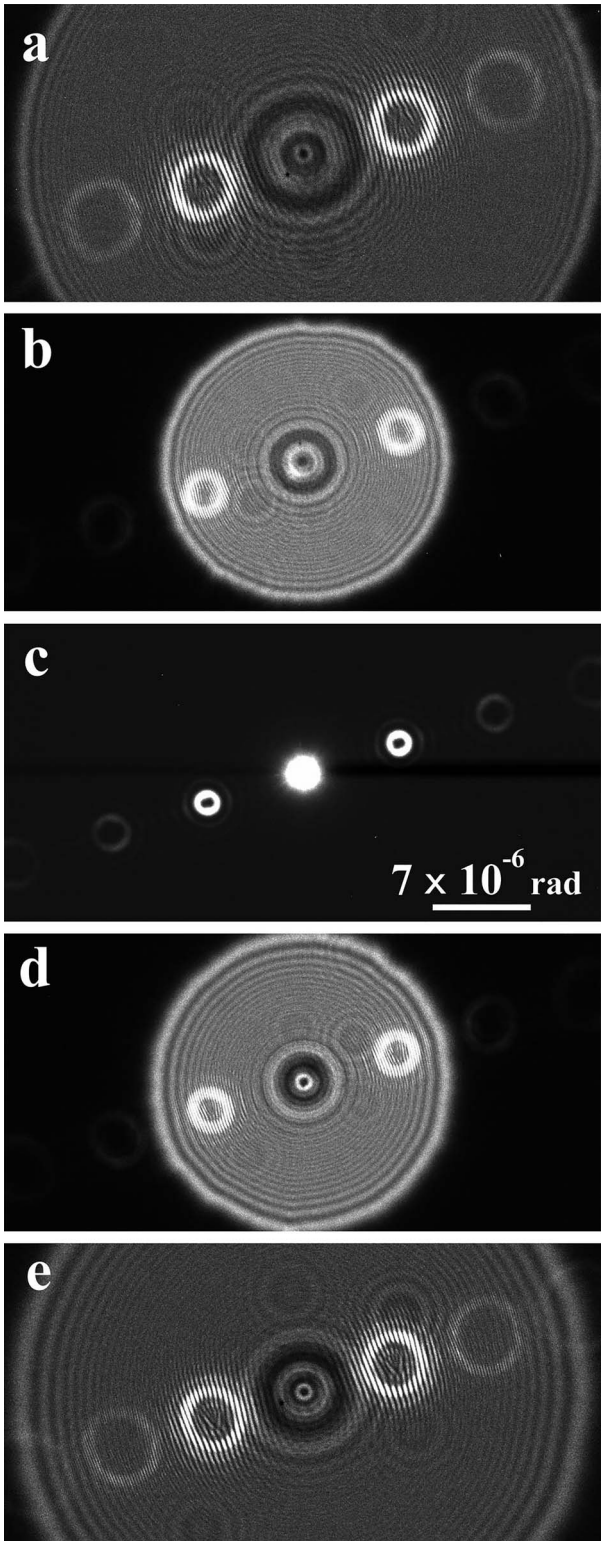

Fig. 3. Diffraction patterns of vortex beams with five focusing conditions Δf; (a) Δf = 39.7 m in underfocus condition, (b) Δf = 23.0 m, (c) Δf = 0 m corresponds to the diffraction patterns, (d) Δf = −16.7 m in overfocus condition and (e) Δf = −35.5 m. The defocusing value Δf is defined as the difference from the camera length of 710 m when observing the diffraction pattern in (c) just on the reciprocal plane.

right-hand side of the reconstructed images as object image and left-hand side images as conjugate images.

The phase gradient and the azimuthal rotation of the vortex structures around the vortex beam of the object image in Fig. 4c can be explained from Fig. 2a and d; the phase distribution in Fig. 4c increases helically in the counter clockwise direction seen from black to white and the helical wavefront moves up in the counter clockwise direction shown in the upper figure of Fig. 2a. The vortex structure around the fan-like reconstructed images shows a clockwise behavior just the same as that of the interference pattern in the lower figure of Fig. 2a. On the other hand, the conjugate image of Fig. 4c corresponds to that of Fig. 2d, which is inverse of image in Fig. 2a. Both the object and conjugate images in Fig. 4c are consistent with the drawings in Fig. 2a and d. Similarly, the phase gradient and the azimuthal rotation of the vortex structures around the vortex beam of the object and conjugate images in Fig. 4d can also be explained from Fig. 2b and c.

The center spots in Fig. 4b–e are modified Airy discs caused by Fraunhofer waves from the opening of the fork-shaped grating, such as the phase difference in each disc is π [6,15], and the diameter of the centered discs is about half of the ordinary circular opening. We confirmed that this change is caused by the annular ring-shaped holograms. In addition, a phase profile of the center spot is similar to that of the Bessel beams [16].

Figures 4b and e show amplitude and phase images from the second order diffraction spots. The phase gradients and the azimuthal rotation of the vortex structures around the vortex beams are explained similarly by using Fig. 2 with twice the amplified phase gradients, so that the topological number is ±6.

In the overfocus holograms in Fig. 5a, which is the same as Fig. 3e, the same arguments used in the explanation of Fig. 4 can be applied in terms of the lensless Fourier transform holography. In Fig. 5a, categorized diffraction spots in red broken squares are drawn for Fig. 5b–e. The upper parts in Fig. 5b–e show reconstructed amplitude images, and the lower parts show reconstructed phase images. Figures 5f and g show composite images of amplitude and phase images for the first and second order diffraction spots. All figures shown in Fig. 5 were recorded and reconstructed in the same procedure as those in Fig. 4. The positions of object and conjugate images in Fig. 5b–e are exchanged from those in Fig. 4, because the angular relation between the vortex beams and the reference wave was exchanged. The phase gradients and the vortex structures of the object and conjugate images in Fig. 5c are explained by using Fig. 2b and c, and the phase gradients and the vortex structures in Fig. 5d are explained by using Fig. 2b and c.

Figure 5b and e show amplitude and the phase images from the second order diffraction spots. The phase gradients and the vortex structures are similarly explained by using Fig. 2 with twice the amplified phase gradients.

Through the above analyses, we have succeeded in recording the lens-less Fourier transform holograms under the underfocus and overfocus conditions. Both holograms are mathematically identical to each other except for defocusing distances in optical conditions. Therefore, the same reconstructed images should be obtained from both holograms as observed in the same reconstructed amplitude images, Fig. 4c and d and Fig. 5c and d.

The upper figures in Fig. 6a–d show the reconstructed phase distributions of the object images in fan-like structures from Figs. 4 and 5, and the lower figures show phase profiles along the red broken circles in the counter clockwise direction. Figure 6a corresponds to the right-hand side of Fig. 4c; Fig. 6b corresponds to the left-hand

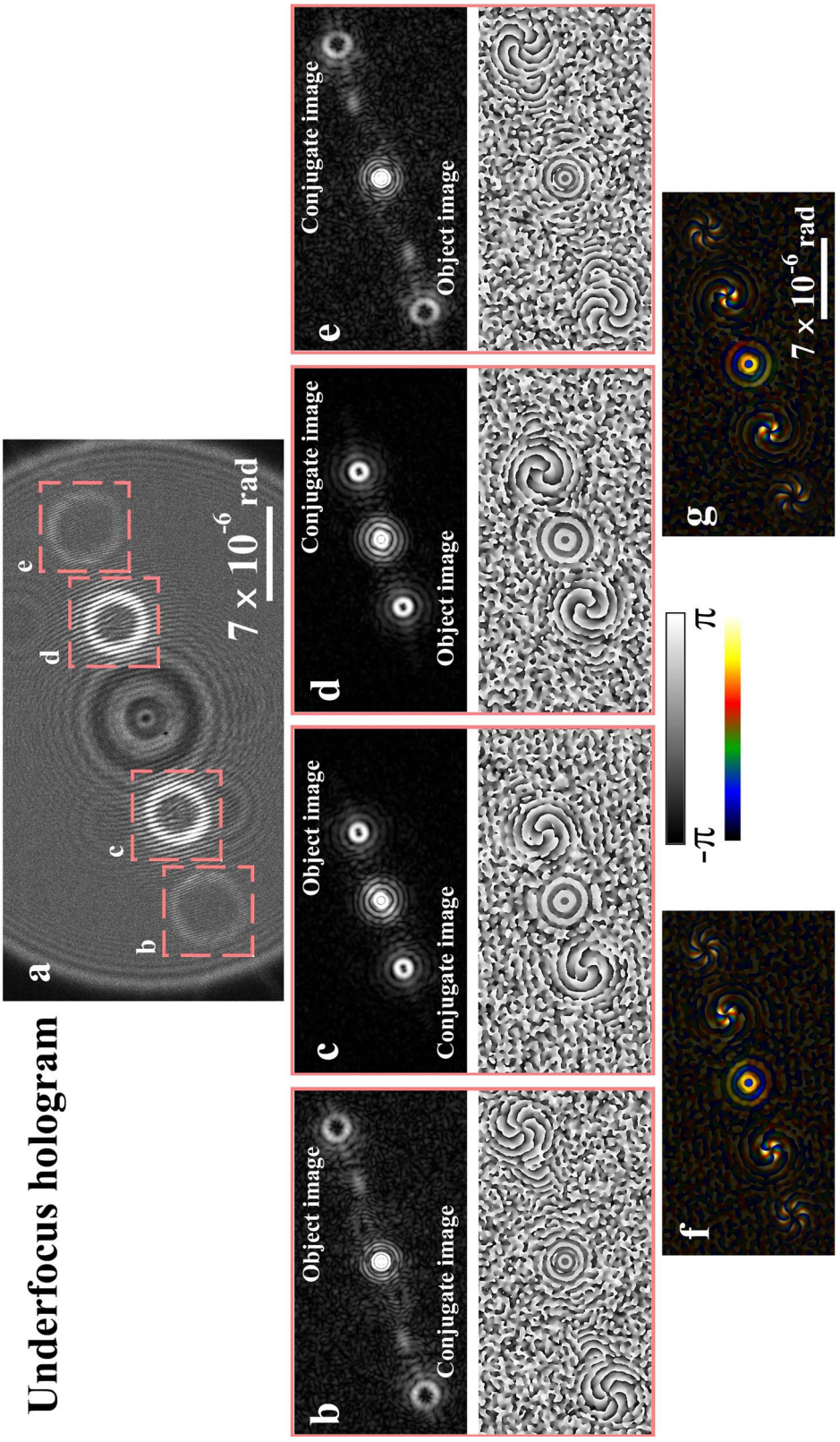

Fig. 4. Lensless Fourier transform holograms and reconstructed images under the underfocus condition: (a) is the same as Fig. 3a with categorized diffraction spots; (b)–(e) show reconstructed amplitude and phase images, and (f) and (g) show composite images of amplitude and phase distributions with the first and second order diffraction waves. The amplitude images are the same as those of the diffraction patterns shown in Fig. 3c. The phase images show fan-like structures of contrast, indicating gradient of the phase distributions.

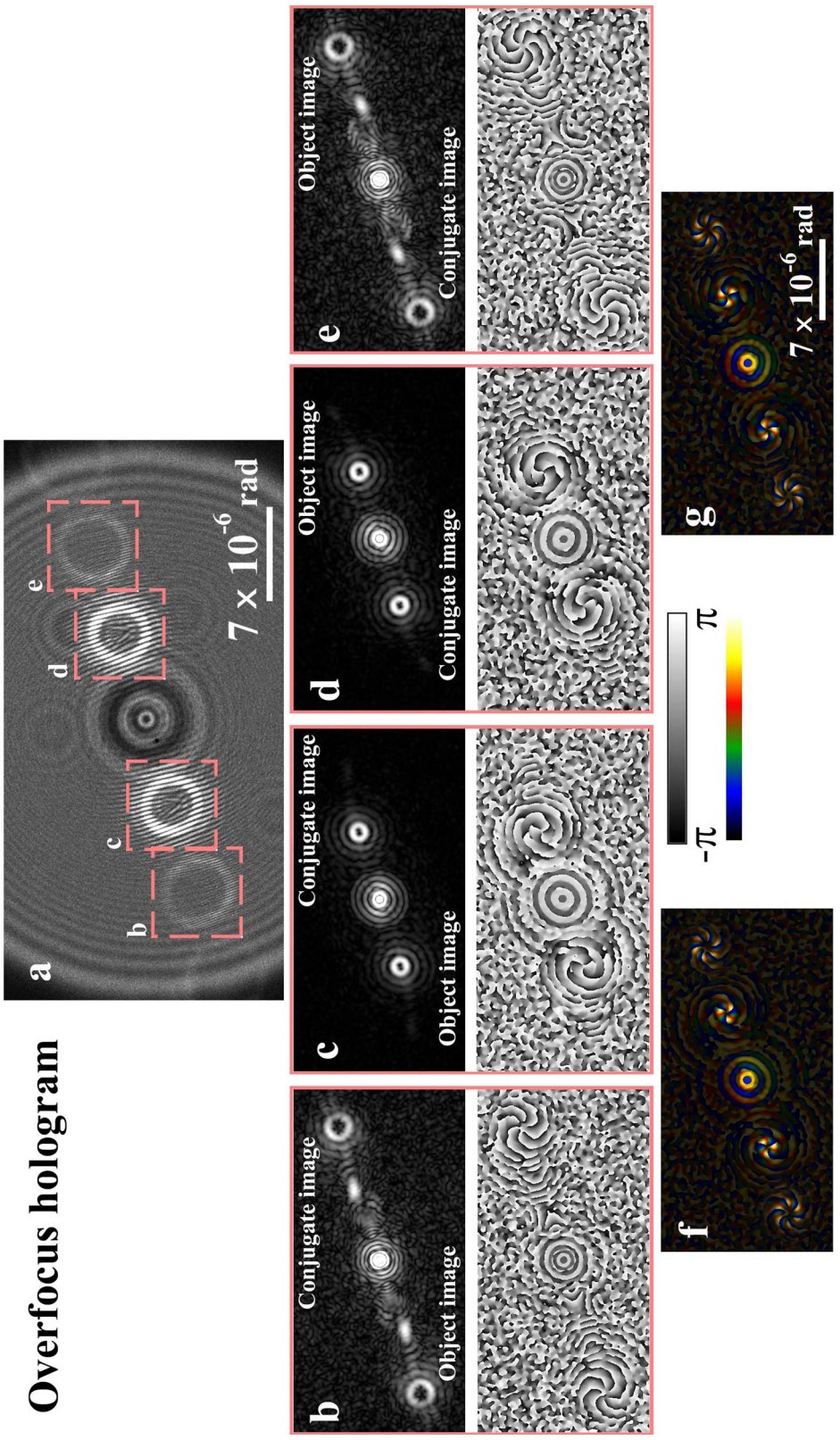

Fig. 5. Lensless Fourier transform holograms and reconstructed images under the overfocus condition: (a) is the same as Fig. 3e; (b)–(e) show reconstructed amplitude and phase images, and (f) and (g) show composite images of amplitude and phase distributions with the first and second order diffraction waves. The phase images show fan-like structures of contrast, indicating gradient of the phase distributions.

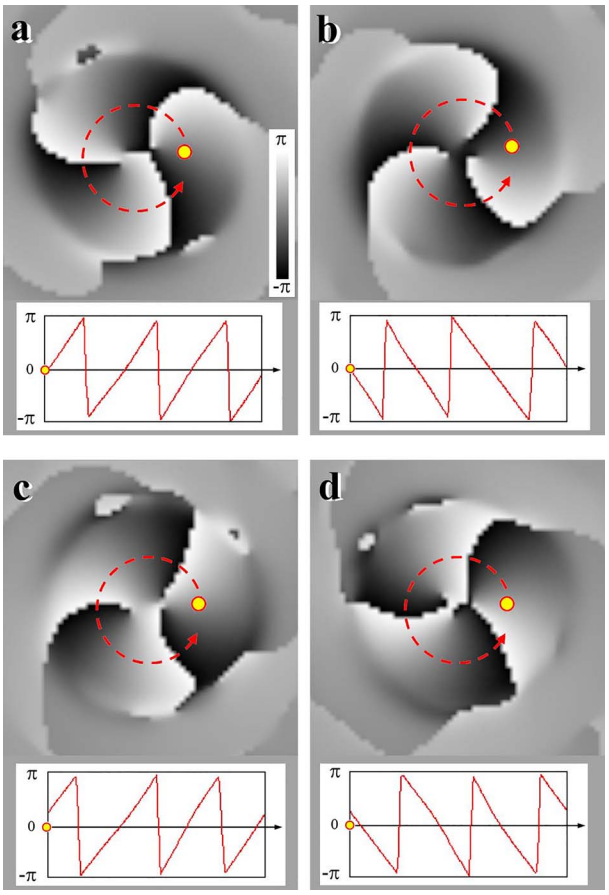

Fig. 6. Reconstructed phase distributions of the object images from Figs. 4 and 5 and phase profiles along the circular red broken lines; (a) the right-hand side of the underfocus hologram of Fig. 4b and c the left-hand side of the underfocus hologram of Fig. 4c and d the left-hand side of the overfocus hologram of Fig. 5c and d the right-hand side of the overfocus hologram of Fig. 5d. Both underfocus and overfocus holograms lead to the same reconstruction images.

side of Fig. 4d. Note that Fig. 6a and b are reconstructed from the underfocus holograms. Figure 6c corresponds to the left-hand side of Fig. 5c; Fig. 6d corresponds to the right-hand side of Fig. 5d. Note that Fig. 6c and d are reconstructed from the overfocus holograms. Phase profiles of Fig. 6a and c are the same and those of Fig. 6b and d are the same. These profiles clearly show that the reconstructed phase distributions from the underfocus and overfocus holograms are the same.

In conclusion, we have developed a lensless Fourier transform holography for the reconstruction of electron vortex beams in the reciprocal plane. The holography formation is the same as that of the electron holography for the vortex beams: two wave interferences between Bragg diffraction waves generated by fork-shaped grating as object waves and the 0^{th} order transmission wave as a reference wave. The underfocus and overfocus holograms at displaced positions away from the reciprocal plane are recorded. Fourier transform as a reconstruction procedure has been performed for four Bragg diffraction waves of both holograms; then, both vortex beams can be reconstructed in amplitude and phase distributions in terms of object and conjugate images. We have confirmed that the developed lens-less Fourier transform holography has an advantage of reconstructing wave properties in the reciprocal space. With this development together with the conventional reconstruction method, electron holography can systematically cover the whole space ranges from the real space to the reciprocal space.

Acknowledgements

We are sincerely grateful to Prof J. Yamasaki of Osaka University for valuable discussions on Fourier transform. We also thank Ms K. Shimada of RIKEN for preparing fork-shaped gratings.

Funding

KAKENHI, Grant-in-Aid for Scientific Research ((B) 18H03475).

References

1. Tonomura A (1999) *Electron holography*, 2nd edn, (Springer, Heidelberg).
2. Harada K, Tonomura A, Togawa Y, Akashi T, and Matsuda T (2004) Double-biprism electron interferometry. *Appl. Phys. Lett.* 84: 3229–3231.
3. Harada K, Akashi T, Togawa Y, Matsuda T, and Tonomura A (2005) Variable interference azimuth-angle in double biprism electron interferometry. *Jpn. J. Appl. Phys.* 44: L636–L639.
4. Murakami Y, Niitsu K, Tanigaki T, Kainuma R, Park H S, and Shindo D (2014) Magnetization amplified by structural disorder within nanometer-scale interference region. *Nat. Comm.* 5: 1–8.
5. Yamamoto K, Iriyama Y, and Hirayama T (2016) Operando observations of solid-state electrochemical reaction in Li-ion batteries by spatially resolved TEM EELS and electron holography. *Microscopy* 66: 50–61.
6. Harada K, Niitsu K, Shimada K, Kodama T, Akashi T, Ono Y A, Shindo D, Shinada H, and Mori S (2019) Electron holography on Fraunhofer diffraction. *Microscopy* 68: 254–260.
7. Leith E N, and Upatnieks J (1964) Wavefront reconstruction with diffused illumination and three-dimensional objects. *J. Opt. Soc. Amer.* 54: 1295–1301.
8. Lauer R (1984) Interferometry by electron Fourier holography. *Optik* 67: 291–293.
9. Endoh H (2009) Fresnel zone plate and X-ray microscope using the Fresnel zone plate. US patent application US2009/0052619A1. Feb. 26, 2009.
10. McMorran B J, Agrawal A, Anderson I M, Herzing A A, Lezec H J, McClelland J J, and Unguris J (2011) Electron vortex beams with high quanta of orbital angular momentum. *Science* 331: 192–195.
11. Harada K, Kohashi T, and Koguchi M (2019) Electron vortex beam and their control. *Mat. Trans.* 60: 2096–2102.
12. Harada K, Shimada K, Ono Y A, Iwasaki Y, Niitsu K, and Shindo D (2018) Electron holography study on vortex beam phases in real space. *Microsc. Microanal.* 24: 1470–1471.
13. Harada K, Shimada K, and Ono Y A (2020) Electron holography for vortex beams. *Appl. Phys. Express* 13: 032003. doi: 10.35848/1822-0786/ab7059.
14. Nakajima H, Kotani A, Harada K, and Mori S (2018) Electron diffraction covering a wide angular range from Bragg diffraction to small-angle diffraction. *Microscopy* 67: 207–213.
15. Born M and Wolf E (1985) *Principles of optics*, 6th edn, Ch 8, 428–435 (Pergamon Press, Oxford, U.K.).
16. Grillo V, Karimi E, Gazzadi G C, Frabboni S, Dennis M R, and Boyd R W (2014) Generation of nondiffracting electron Bessel beams. *Phys. Rev. X* 4: 1–7.